^{18}F-ML-10, a PET Tracer for Apoptosis: First Human Study

Johanna Höglund*[1], Anat Shirvan*[2], Gunnar Antoni[3], Sven-Åke Gustavsson[4], Bengt Långström[5], Anna Ringheim[1], Jens Sörensen[3], Miri Ben-Ami[2], and Ilan Ziv[2]

[1]Uppsala Imanet AB, GE Healthcare, Uppsala, Sweden; [2]Aposense Ltd., Petach Tikva, Israel; [3]Department of Radiology, Oncology and Radiation Sciences, Uppsala University, Uppsala, Sweden; [4]Uppsala University Hospital, Uppsala, Sweden; and [5]Department of Biochemistry and Organic Chemistry, Uppsala University, Uppsala, Sweden

Clinical PET of apoptosis may have substantial value in advancing patient care. We report here the first-in-humans study with ^{18}F-labeled 2-(5-fluoropentyl)-2-methyl malonic acid (^{18}F-ML-10), a small-molecule PET tracer for apoptosis. Presented are the dosimetry, biodistribution, stability, and safety profiles of this PET tracer in healthy human volunteers. Also reported is tracer binding to targeted apoptotic cells in testicular tissue, where a relative abundance of apoptotic cells is normally observed. **Methods:** ^{18}F-ML-10 (233 ± 90 MBq) was intravenously administered to 8 healthy subjects, followed by whole-body PET/CT for 220 min. Serial blood and urine samples were collected for radioactivity measurement, and plasma tracer stability was assessed by high-performance liquid chromatography. Dosimetry calculations were performed using OLINDA/EXM software. **Results:** ^{18}F-ML-10 manifested high stability in vivo and rapid distribution followed by fast clearance, with an elimination half-life of 1.3 ± 0.1 and 1.1 ± 0.2 h from the blood and from all other organs, respectively, and excretion through the urine. Dosimetry showed an average effective whole-body dose of 15.4 ± 3.7 μSv/MBq, with the urinary bladder being the dose-limiting organ. Selective accumulation and retention of the tracer in the testes was observed in all male subjects, a finding also demonstrated in mice using both small-animal PET and histopathology, confirming binding to apoptotic cells. Administration of ^{18}F-ML-10 was safe, without adverse effects. **Conclusion:** ^{18}F-ML-10 administered to healthy humans demonstrated a favorable dosimetry, biodistribution, stability, and safety profile. Binding to apoptotic sites was also demonstrated. These data support further development of this small-molecule probe for clinical PET of apoptosis.

Key Words: molecular imaging; apoptosis; PET; dosimetry; biodistribution

J Nucl Med 2011; 52:720–725
DOI: 10.2967/jnumed.110.081786

Apoptosis is a fundamental biologic process of regulated cell death, having a role in numerous medical disorders. Accordingly, noninvasive imaging of apoptosis may be valuable in future clinical care for diagnosis of disease, monitoring of disease course, evaluation of treatment efficacy, or assistance in drug development.

Annexin-V (*1*), synaptotagmin (*2*), caspase inhibitors (*3*), and hydrophobic cations (*4*) have been explored as potential probes for imaging apoptosis. SPECT with technetium-labeled annexin-V has also been tested in the clinical setting (*5*). Although PET emerges as the leading modality for molecular imaging, no PET tracer for apoptosis is currently available for clinical use (*6*).

^{18}F-labeled 2-(5-fluoropentyl)-2-methyl malonic acid (^{18}F-ML-10; molecular weight, 206) is an ^{18}F-labeled small-molecule probe for PET, derived from the Aposense (Aposense Ltd.) family of biomarkers for apoptosis (*7*). Aposense compounds are rationally designed to selectively bind and accumulate in cells manifesting apoptosis-specific alterations, collectively designated the apoptotic membrane imprint (*8*), comprising acidification of the external membrane leaflet due to exposure of phosphatidylserine, permanent membrane depolarization, irreversible loss of intracellular pH control, and activation of the phospholipid scrambling mechanism while membrane integrity is still preserved. The concurrence of these apoptotic membrane imprint features marks the commitment point of a cell to the apoptotic death process, thus distinguishing such a cell from its viable or necrotic counterparts (*8*). In preclinical models, ^{18}F-ML-10 manifested selective binding to apoptotic cells, high stability, and a favorable biodistribution profile on systemic administration in vivo (*8,9*), thus supporting the advancement of this probe into clinical development.

We present the first clinical study with ^{18}F-ML-10, performed on healthy volunteers, to evaluate the dosimetry, biodistribution, stability, and safety of this probe. To demonstrate binding of the tracer to targeted apoptotic cells, we also analyzed uptake of ^{18}F-ML-10 in testicular tissue because of its relative abundance of apoptotic cells and its use of apoptosis as a physiologic quality control mechanism during normal spermatogenesis (*10*).

MATERIALS AND METHODS

Human Subjects

The study (EudraCT 2006-001288-4), which took place at the Uppsala Imanet PET Center, was approved by the Swedish Medical Products Agency, the Radiation Safety Committee, and the

Received Aug. 27, 2010; revision accepted Feb. 16, 2011.
For correspondence or reprints contact: Gunnar Antoni, Department of Radiology, Oncology, and Radiation Sciences, Uppsala University, SE-751 85 Uppsala, Sweden.
E-mail: gunnar.antoni@onkologi.uu.se
*Contributed equally to this work.

local Independent Ethics Committee and was performed according to the good-clinical-practice guidelines of the International Conference on Harmonisation of Technical Requirements for Registration of Pharmaceuticals for Human Use. Four men and 4 women (mean age ± SD, 23 ± 3 and 33 ± 10 y, respectively; range, 21–44 y; weight, 69 ± 11 kg) were enrolled. All provided written informed consent and were confirmed to be healthy by medical history, physical examination, routine laboratory tests, urine drug screening, negative pregnancy test when applicable, and electrocardiography.

Animals

For small-animal PET and histologic studies, male BALB/c mice (8 wk old) were obtained from Harlan Laboratories. Animal studies were performed according to the Guiding Principles for Research Involving Animals and were approved by the local Animal Care Committee.

Labeling of ^{18}F-ML-10

Radiolabeling of ML-10 with ^{18}F was performed from the respective ML-10 precursor as previously described (*9*). A precursor standard of ML-10 and D-ML-10 (the fluorescent, dansyl-labeled ML-10 analog) was supplied by Albany Molecular Research. Other chemicals were obtained from commercial sources and were of analytic grade. The radiochemical purity of ^{18}F-ML-10 was more than 97%.

PET/CT Procedure

^{18}F-ML-10 was administered intravenously at a dose of 233 ± 90 MBq and a tracer mass of less than 8 μg/person. The subjects fasted for at least 6 h before tracer administration. The principal investigator ensured adequate hydration in all subjects, including intravenous administration of glucose solution (25 mg/mL, 5−10 mL/kg/h) to 6 subjects before ^{18}F-ML-10 administration. Immediately (0−2 min) after tracer injection, whole-body PET/CT was initiated using a Discovery ST scanner (GE Healthcare). The acquisition was performed in 2-dimensional mode, yielding a 15.7-cm axial and 70-cm transaxial field of view. Scatter correction, random counts, and dead-time correction were incorporated into the inbuilt reconstruction algorithm of the scanner. PET data were reconstructed using ordered-subsets expectation maximization (2 iterations; 30 subsets). The protocol included 3 PET/CT sessions spanning a maximum of 220 min, with each session consisting of 6–8 bed positions covering the torso and the head. Session 1 consisted of 6–8 examinations at 60 s/bed position; session 2, 2 examinations at 240 s/bed position; and session 3, 1–2 examinations at 240–480 s/bed position. Each session was initiated by a transmission CT scan (140 kV; 10–20 mAs). The subjects were permitted to rise and move between sessions and were encouraged to void to enhance tracer clearance.

Blood and Urine Sampling

Venous blood samples for radioactivity measurements were collected at 0.5, 1, 2, 5, 10, 20, 30, 45, 90, 120, 150, 180, and 220 min after ^{18}F-ML-10 injection, to generate blood time–activity curves and to calculate biologic half-life. For metabolite analysis, plasma samples were collected at 5, 30, 90, and 150 min after tracer injection and were centrifuged (3,100*g* at 4°C for 3 min). Aliquots of 2 × 0.6 mL were analyzed as previously described (*9*). Urine was collected for measurement of ^{18}F radioactivity at 59 ± 2, 134 ± 5, and 205 ± 5 min after tracer administration.

Image Analysis

Images were analyzed using a Gold 2.10 system (Hermes Medical Solutions). For each subject, regions of interest of similar size and shape were outlined on the CT images and copied onto the PET images. For generation of time–activity curves, regions of interest were drawn over major organs (i.e., liver, spleen, kidney, pancreas, lung, heart wall, brain, muscle, bone, and testis) and transferred to the PET images. Data were decay-corrected from the time of ^{18}F-ML-10 administration. For each region, standardized uptake values were calculated, allowing interindividual comparison.

Dosimetry

Dosimetry calculations were performed using the software OLINDA/EXM (*11*). Residence time for each organ was calculated from the non–decay-corrected time–activity curve data. A standard body weight (56.9-kg woman and 73.7-kg man) and standard organ weights, as suggested by the OLINDA/EXM software, were used for data standardization. For calculation of the residence time of the urinary bladder contents, a dynamic bladder model was used, according to Cloutier et al. (*12*).

Safety

All subjects were monitored for safety parameters from the time of ^{18}F-ML-10 administration until the end of the final PET/CT session (220 min after injection) and again at 3 ± 1 d after tracer administration via interview, electrocardiography, and measurements of heart rate, blood pressure, respiratory rate, and body temperature. In addition, clinical laboratory blood and urine tests were performed before and after administration of ^{18}F-ML-10.

Small-Animal PET Studies and Histologic Assessment of Testicular Uptake of ^{18}F-ML-10 in Mice

Each mouse was injected with 20 MBq of ^{18}F-ML-10 and subjected to a 120-min scan using an HRRT PET scanner (Siemens/CTI) under 0.5%–1% isoflurane anesthesia. Static summed images between 30 and 60 min after injection were created for visualization of tracer uptake and were interpreted qualitatively. For histologic studies, each mouse was injected intravenously with ML-10 labeled with a fluorophore (dansyl; D-ML-10, 140 mg/kg). One hour later, after sacrifice of the animals, testes were excised and subjected to fluorescent histopathologic assessment, using a BX51 microscope (Olympus Optical Co.) equipped with a UMNU2 filter. Consecutive slides were visualized for apoptotic nuclear fragmentation using deoxyuride-5′-triphosphate biotin nick end labeling (TUNEL) (ApopTag fluorescein direct kit, S7160; Intergen).

Statistical Analysis

For each quantitative parameter, mean values and SD were calculated (Statistica, version 7; StatSoft). Intergroup statistical significance ($P < 0.05$) was evaluated using the Wilcoxon rank sum test.

RESULTS

Tracer Stability on Administration In Vivo

The in vivo stability of ^{18}F-ML-10 in plasma was monitored during the first 150 min after its intravenous administration (Fig. 1). A major peak corresponding to intact ^{18}F-ML-10 and a minor peak indicating a metabolite were observed. The minor peak, which was more polar than

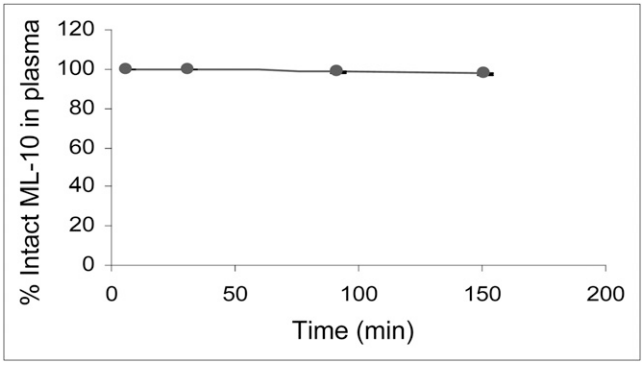

FIGURE 1. Stability of ^{18}F-ML-10 in vivo in plasma of healthy humans. Intact ^{18}F-ML-10 was measured in all 8 subjects at different time points (up to 150 min) after administration. Data are mean percentage (±SD) of total radioactivity (error bars were too small to be visualized).

^{18}F-ML-10, was not ^{18}F, thus indicating that the tracer does not undergo defluorination in vivo. ^{18}F-ML-10 therefore manifested high stability in vivo, with 97.5% ± 0.4% of the tracer still intact 150 min after administration.

Biodistribution

After its intravenous administration, ^{18}F-ML-10 was initially detected in the blood compartment and then rapidly distributed through the extracellular space, followed by quick excretion through the kidneys to the urine. Radioactivity was already detectable in the urinary bladder at 10 min after tracer administration. Tracer uptake images at various time points from a representative subject are shown in Figure 2. Time–activity data were generated for various organs (Fig. 3). ^{18}F-ML-10 showed rapid clearance from nontarget organs, with an elimination half-life of 1.3 ± 0.1 h for the blood and 1.1 ± 0.2 h for all other organs. The kinetics of ^{18}F-ML-10 exhibited similar patterns in all organs (except the testes), closely following the blood kinetics and consistent with the extracellular distribution of the probe. Intersubject variability in uptake and biologic half-lives was minimal, and the biodistribution profiles did not differ between men and women.

The magnitude of uptake differed between various organs, reflecting the organ-specific blood pool. Furthermore, the organ-to-blood standardized uptake value ratio gave almost constant values from 30 min after tracer administration, indicating that tracer clearance rate from various organs paralleled that from the blood. This finding further supports the likelihood that ^{18}F-ML-10 is mainly distributed in the extracellular space. High values in kidneys seem to reflect urinary excretion of the tracer rather than retention of ^{18}F-ML-10 in renal tissue.

In all 4 male subjects, a distinct pattern of ^{18}F-ML-10 uptake was observed in the testes, characterized by a gradual increase in uptake after tracer administration, a peak at around 25 min, a plateau for up to 90 min, and a slow decrease thereafter. Concurrently, the tracer cleared from the blood and from all surrounding tissues (e.g., bone or muscle), thereby resulting in selective hot spots in the testes on the PET/CT image (Fig. 4A). Signal intensity was 5-fold higher in the testes than in muscle.

Dosimetry

The fraction of radioactivity excreted at the end of the PET session (220 min after ^{18}F-ML-10 administration) was calculated from the total administered radioactivity. The total excreted radioactivity per individual was 72% ± 5%. Organ and effective whole-body doses for each individual were calculated using the estimates of the model parameters (Table 1). The urinary bladder wall had the highest dose of ^{18}F-ML-10, 172 ± 18.8 μSv/MBq, and was therefore the dose-limiting organ. When voiding frequencies in the OLINDA bladder model were changed from once every 3 h to once every hour, the dose to the urinary bladder was decreased by a factor of 2.8. The mean effective whole-body radiation dose related to ^{18}F-ML-10 administration was 15.4 ± 3.7 μSv/MBq.

Selective Uptake of ^{18}F-ML-10 by Apoptotic Cells in Testes of Mice

To demonstrate binding of ML-10 to apoptotic cells in the testes, we performed small-animal PET and a correlative histologic study on male mice. Similar to the observation in

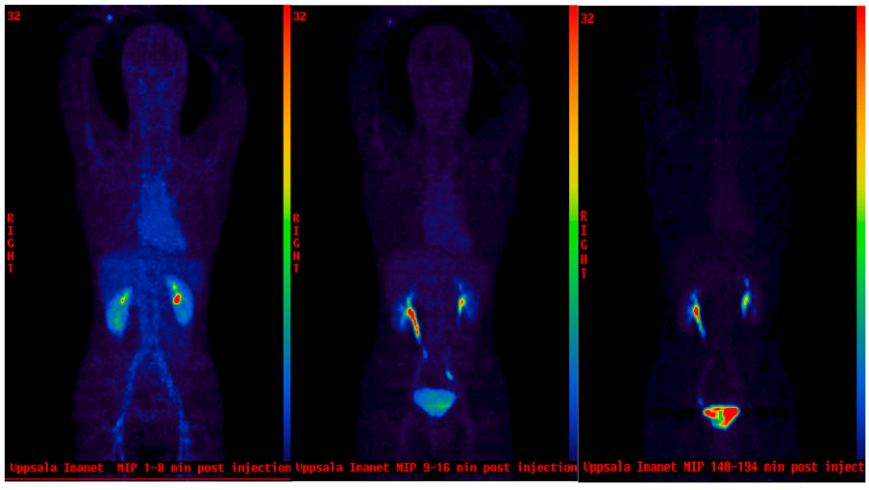

FIGURE 2. Whole-body PET images of biodistribution and clearance of ^{18}F-ML-10 in healthy volunteer. Whole-body PET images of ^{18}F-ML-10 uptake in representative subject were acquired over 7 or 8 bed positions of varying duration. Images of whole body were obtained during minutes 0–8 at 60 s per bed position (left), minutes 9–16 at 60 s per bed position (middle), and minutes 149–194 at 6 min per bed position (right). ^{18}F-ML-10 was initially detected in vascular compartment, then rapidly distributed through extracellular space, and finally was rapidly excreted through urine.

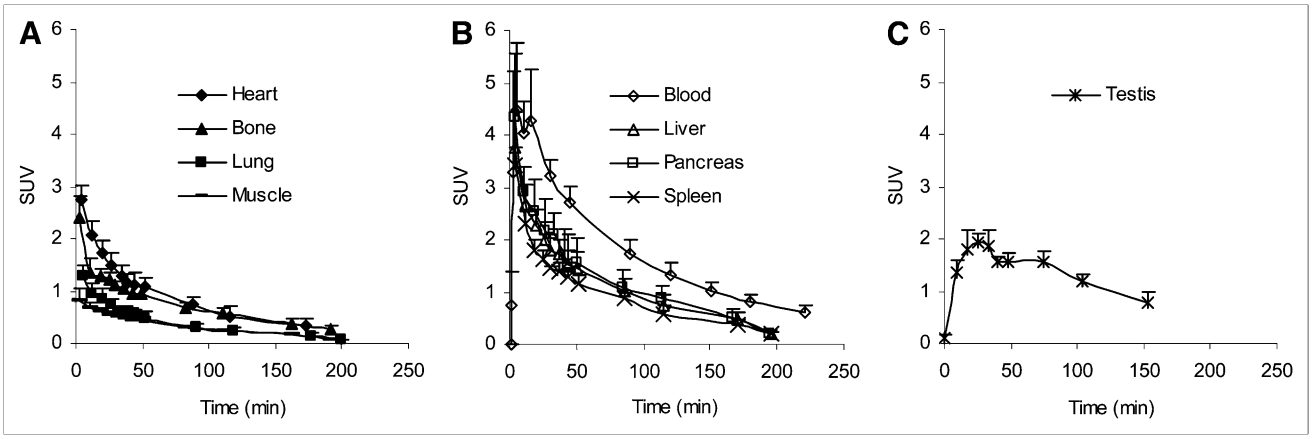

FIGURE 3. Time–activity curves for ^{18}F-ML-10. Time–activity data were generated for several organs at various time points during the 220 min after intravenous tracer administration. Data are mean + SD for $n = 8$ (A and B) and $n = 4$ (C).

humans, hot spots were revealed in the testes, corresponding to selective accumulation of ^{18}F-ML-10 (Fig. 4B). In addition, fluorescent microscopy studies were performed in which the fluorescent D-ML-10 was injected intravenously, the animals were sacrificed, and cryosections of the testicular tissue were prepared. Selective uptake of the probe into specific testicular cells was observed, predominantly at the periphery of the seminiferous tubules. That these cells were apoptotic was then confirmed by histologic TUNEL staining, which detected the characteristic apoptotic DNA fragmentation (Fig. 4C).

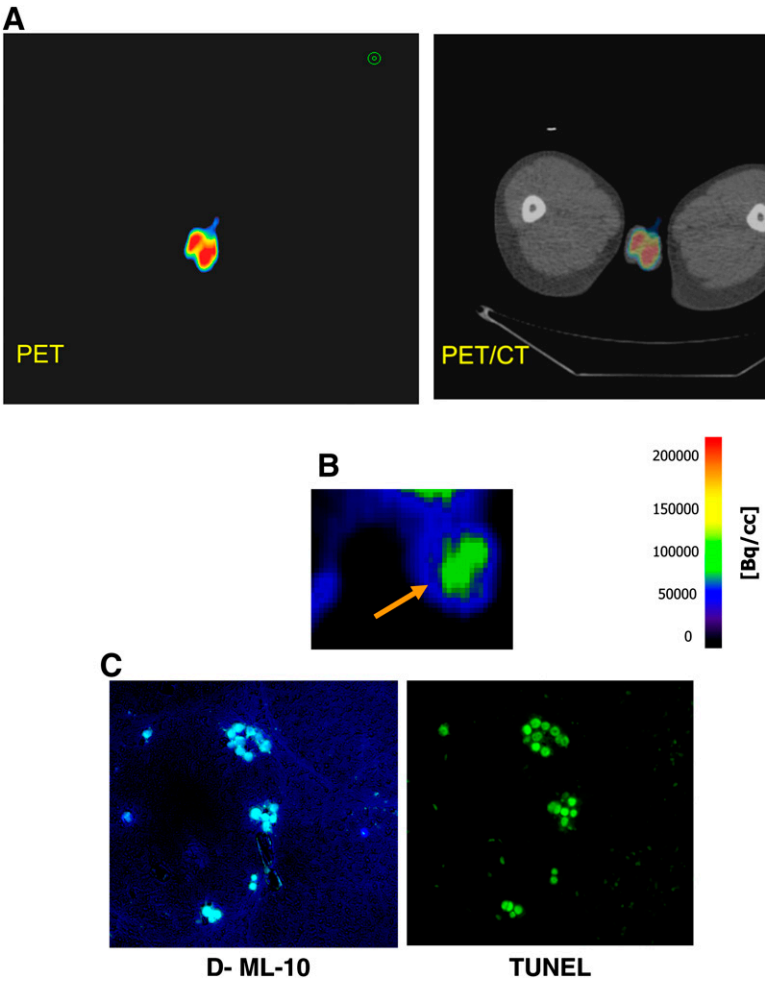

FIGURE 4. Testicular uptake of ^{18}F-ML-10 as shown in PET images and correlative study in mice. (A) PET image of ^{18}F-ML-10 (summation of minutes 76–80, left) and fusion of CT and PET images (right) at level of testes show findings in representative healthy human. (B) Small-animal PET static image of ^{18}F-ML-10 in male mouse shows selective uptake in testes. (C) Fluorescent microscopy image of testicular tissue of mouse shows selective uptake of D-ML-10 (left) and respective TUNEL staining for apoptotic DNA fragmentation (right), confirming that cells manifesting ML-10 uptake were indeed undergoing apoptosis.

TABLE 1
Radiation Dosimetry Data of ^{18}F-ML-10: Organ Doses and Effective Whole-Body Dose

Target organ	Organ dose (10^{-3} mSv/MBq)
Adrenals	10.9 ± 4.0
Brain	0.8 ± 0.2
Breasts	1.0 ± 2.1
Gallbladder wall	4.0 ± 0.9
Lower large intestine wall	6.0 ± 1.0
Small intestine	3.5 ± 0.7
Stomach wall	2.4 ± 0.6
Upper large intestine wall	3.1 ± 0.6
Heart wall	13.8 ± 2.9
Kidney	39.5 ± 14.7
Liver	11.8 ± 3.3
Lungs	3.2 ± 0.7
Muscle	4.4 ± 1.0
Pancreas	11.6 ± 3.3
Red marrow	3.1 ± 0.7
Osteogenic cells	3.5 ± 1.0
Skin	1.3 ± 0.2
Spleen	9.6 ± 2.7
Thymus	2.0 ± 0.3
Thyroid	1.1 ± 0.2
Urinary bladder wall	172 ± 18.8
Ovaries	24.2 ± 6.8
Uterus	11.8 ± 1.7
Testes	10.9 ± 1.4
Total body	3.6 ± 0.7

Data are mean ± SD. Effective whole-body dose is 15.4 ± 3.7 μSv/MBq.

Safety

No adverse effects associated with ^{18}F-ML-10 administration were detected in any participating subject in the study. All measured vital signs, including heart rate, blood pressure, respiratory rate, body temperature, and the electrocardiogram, remained stable throughout the study, and no significant changes were observed in any of the measured parameters during the PET/CT sessions or at a follow-up visit 3 d after administration.

DISCUSSION

In this report, we have presented the results of the first-in-humans study with ^{18}F-ML-10, a small-molecule PET tracer for apoptosis. ^{18}F-ML-10, derived from the Aposense family of small-molecule probes for apoptosis (*6,8,9*), was rationally designed to accommodate the challenging set of features required of a useful PET tracer for clinical practice. An important finding of the study was the high stability of the probe in vivo, with 97.5% ± 0.4% of tracer intact at 150 min after administration (Fig. 1). Such high stability ensures that the measured radioactivity throughout the imaging period indeed originates from the intact tracer, alleviating the need to correct for signals from metabolites or to consider potential molecular interactions of metabolites.

One prerequisite of a probe for apoptosis is lack of binding to viable cells and tissues. Therefore, in healthy subjects, the tracer should manifest largely extracellular distribution. Indeed, this was the profile observed with ^{18}F-ML-10. The tracer exhibited uniform distribution through the extracellular space, and the pattern of organ uptake and clearance followed monoexponential blood kinetics. Washout half-life from various organs was the same as the clearance rate from the blood (i.e., about 1 h; Fig. 3), and elimination was through the urine (Fig. 2).

For dosimetry calculations, each subject underwent multiple whole-body PET/CT examinations as previously described (*13–15*), generating datasets of 9–11 time points per organ per individual over a period of 220 min. Subsequently, regions of interest were outlined on the diagnostic CT images, resulting in subject-specific time–activity curves and, hence, individual dose estimates. The mean effective whole-body dose calculated by the OLINDA/EXM software for the study subjects was 15.4 ± 3.7 μSv/MBq of ^{18}F-ML-10. Calculated values were slightly higher for women (18.5 ± 2.4 μSv/MBq) than for men (12.4 ± 0.9 μSv/MBq), as may be attributed to intersex differences in physics (e.g., body volume, body surface area, or distance between organs) considered in the OLINDA/EXM algorithm, glomerular filtration rate, or age (*16*). No differences in biodistribution parameters or the biologic half-lives of the tracer were observed between men and women. These values of effective whole-body dose are below the recommended Food and Drug Administration limit for research studies not under an investigational new drug application (*17*). Because of the exclusion of ^{18}F-ML-10 from viable cells, its distribution in the extracellular space, and subsequent urinary excretion, the urinary bladder was found to be the dose-limiting organ, with a mean dose of 172 ± 18.8 μSv/MBq. Such a pattern is also observed with, for example, the PET tracers ^{18}F-fluorothymidine (*18*) and ^{18}F-galacto-RGD (*19*). As is customary for studies of probes that are excreted through the urine, our subjects received adequate hydration and were encouraged to urinate frequently between PET sessions. The dosimetry data obtained in the present study were acceptable to the Swedish Medical Products Agency and the radiation safety committee, allowing us to proceed to the second part of the study—that is, on patients with acute cerebral stroke (manuscript in preparation). The effective whole-body dose was 15.4 ± 3.7 μSv/MBq, which is comparable to or lower than the dose reported for clinically used radiotracers (*13,18–21*).

Apoptosis is known to play an important role in testicular physiology. Because of the importance of adequate spermatogenesis for the integrity of future generations of the species, apoptosis is continuously used as a powerful quality assurance tool to eliminate defective germ cells. Consequently, between 5% and 10% of apoptotic germ cells can normally be observed in histologic studies of testes of young adult men (*10,22*). Interestingly, uptake of ^{18}F-ML-10 reflected this physiologic phenomenon.

Unlike any other examined organ, the testes of all male volunteers demonstrated a 3-phase process in the time–

activity curve: a slow net accumulation, retention, and slow elimination (Fig. 3C). This sequence translated to hot spots in the testes on PET images (Fig. 4A). Parallel studies performed on mice with small-animal PET further supported selective binding of ^{18}F-ML-10 to apoptotic cells in testicular tissue. These studies also included a histologic examination using the fluorescent derivative D-ML-10, through which cells manifesting probe uptake were indeed confirmed to be apoptotic by a correlation with TUNEL staining for apoptotic DNA fragmentation (Figs. 4B and 4C).

These observations of the imaging of physiologic apoptosis are also consistent with the preclinical profile of ML-10 in detection of apoptosis in disease states. Studies of the probe (or its close analog ML-9) have demonstrated its ability to detect apoptosis in various experimental models of disease, both in vitro (*8*) and in vivo; in models of neurovascular cell death in cerebral stroke (*9*); and in chemotherapy-induced apoptosis in tumors (*23*).

Because apoptosis has been shown to play an important role in various medical disorders, detection of apoptosis in vivo may serve as a useful tool in clinical practice, potentially assisting in the diagnosis of disease, the monitoring of disease course, and the assessment of treatment efficacy or serving as a surrogate tool for drug development. The performance of ^{18}F-ML-10, as observed in the present study, encourages further development of this small-molecule PET probe for apoptosis. Its potential future integration into clinical practice may help address these substantial unmet clinical needs.

CONCLUSION

To the best of our knowledge, this is the first report on PET imaging of a small-molecule probe for apoptosis in humans. In this study, ^{18}F-ML-10, a compact ^{18}F-labeled member of the Aposense family, was administered to healthy humans. The observed profile of this probe with respect to biodistribution, dosimetry, safety, stability in vivo, and imaging of physiologic apoptosis supports its further clinical development as a step toward its potential future integration into clinical practice.

DISCLOSURE STATEMENT

The costs of publication of this article were defrayed in part by the payment of page charges. Therefore, and solely to indicate this fact, this article is hereby marked "advertisement" in accordance with 18 USC section 1734.

ACKNOWLEDGMENT

We thank Dr. Avi Cohen for performing the animal studies. The study was financially supported by Aposense Ltd.

REFERENCES

1. Yagle KJ, Eary JF, Tait JF, et al. Evaluation of ^{18}F-annexin V as a PET imaging agent in an animal model of apoptosis. *J Nucl Med.* 2005;46:658–666.
2. Zhu X, Li Z, Zhao M. Imaging acute cardiac cell death: temporal and spatial distribution of ^{99m}Tc-labeled C2A in the area at risk after myocardial ischemia and reperfusion. *J Nucl Med.* 2007;48:1031–1036.
3. Chen DL, Zhou D, Chu W, et al. Comparison of radiolabeled isatin analogs for imaging apoptosis with positron emission tomography. *Nucl Med Biol.* 2009; 36:651–658.
4. Madar I, Huang Y, Ravert H, et al. Detection and quantification of the evolution dynamics of apoptosis using the PET voltage sensor ^{18}F-fluorobenzyl triphenyl phosphonium. *J Nucl Med.* 2009;50:774–780.
5. Kartachova M, van Zandwijk N, Burgers S, van Tinteren H, Verheij M, Valdés Olmos RA. Prognostic significance of ^{99m}Tc Hynic-rh-annexin V scintigraphy during platinum-based chemotherapy in advanced lung cancer. *J Clin Oncol.* 2007;25:2534–2539.
6. Tait JF. Imaging of apoptosis. *J Nucl Med.* 2008;49:1573–1576.
7. Reshef A, Shirvan A, Akselrod-Ballin A, Wall A, Ziv I. Small-molecule biomarkers for clinical PET imaging of apoptosis. *J Nucl Med.* 2010;51:837–840.
8. Cohen A, Shirvan A, Levin G, Grimberg H, Reshef A, Ziv I. From the Gla domain to a novel small-molecule detector of apoptosis. *Cell Res.* 2009;19: 625–637.
9. Reshef A, Shirvan A, Waterhouse RN, et al. Molecular imaging of neurovascular cell death in experimental cerebral stroke by PET. *J Nucl Med.* 2008;49:1520–1528.
10. Martincic DS, Virant Klun I, Zorn B, Vrtovec HM. Germ cell apoptosis in the human testis. *Pflugers Arch.* 2001;442(suppl 1):R159–R160.
11. Stabin MG, Sparks RB, Crowe E. OLINDA/EXM: the second-generation personal computer software for internal dose assessment in nuclear medicine. *J Nucl Med.* 2005;46:1023–1027.
12. Cloutier RJ, Smith SA, Watson EE, Snyder WS, Warner GG. Dose to the fetus from radionuclides in the bladder. *Health Phys.* 1973;25:147–161.
13. Koole M, Lewis DM, Buckley C, et al. Whole-body biodistribution and radiation dosimetry of ^{18}F-GE067: a radioligand for in vivo brain amyloid imaging. *J Nucl Med.* 2009;50:818–822.
14. O'Keefe GJ, Saunder TH, Ng S, et al. Radiation dosimetry of beta-amyloid tracers ^{11}C-PiB and ^{18}F-BAY94-9172. *J Nucl Med.* 2009;50:309–315.
15. Beauregard JM, Croteau E, Ahmed N, van Lier JE, Benard F. Assessment of human biodistribution and dosimetry of 4-fluoro-11β-methoxy-16α-^{18}F-fluoroestradiol using serial whole-body PET/CT. *J Nucl Med.* 2009;50: 100–107.
16. Levey AS, Bosch JP, Lewis JB, Greene T, Rogers N, Roth D. A more accurate method to estimate glomerular filtration rate from serum creatinine: a new prediction equation. Modification of Diet in Renal Disease Study Group. *Ann Intern Med.* 1999;130:461–470.
17. Title 21 of *Code of Federal Regulations* part 361.1: Radioactive drugs for certain research uses. Available at: http://www.accessdata.fda.gov/scripts/cdrh/cfdocs/cfcfr/CFRSearch.cfm?fr=361.1. Accessed March 25, 2011.
18. Vesselle H, Grierson J, Peterson LM, Muzi M, Mankoff DA, Krohn KA. ^{18}F-fluorothymidine radiation dosimetry in human PET imaging studies. *J Nucl Med.* 2003;44:1482–1488.
19. Beer AJ, Haubner R, Wolf I, et al. PET-based human dosimetry of ^{18}F-galacto-RGD, a new radiotracer for imaging αvβ3 expression. *J Nucl Med.* 2006;47:763–769.
20. Nye JA, Schuster DM, Yu W, Camp VM, Goodman MM, Votaw JR. Biodistribution and radiation dosimetry of the synthetic nonmetabolized amino acid analogue anti-^{18}F-FACBC in humans. *J Nucl Med.* 2007;48:1017–1020.
21. Hays MT, Watson EE, Thomans SR, Stabin M. MIRD dose estimate report no. 19: radiation absorbed dose estimates from ^{18}F-FDG. *J Nucl Med.* 43: 210–214.
22. Hassan A, el-Nashar EM, Mostafa T. Programmed cell death in varicocele-bearing testes. *Andrologia.* 2009;41:39–45.
23. Grimberg H, Levin G, Shirvan A, et al. Monitoring of tumor response to chemotherapy in vivo by a novel small-molecule detector of apoptosis. *Apoptosis.* 2009;14:257–267.